Analysis of airborne-derived sea ice emissivities up to 340 GHz in preparation for future satellite missions

Nils Risse[1], M. Mech[1], C. Prigent[2], G. Spreen[3], and S. Crewell[1]

[1] Institute for Geophysics and Meteorology, University of Cologne
[2] Laboratoire d'Etudes du Rayonnement et de la Matière en Astrophysique et Atmosphères, Observatoire de Paris, CNRS
[3] Institute of Environmental Physics, University of Bremen

Get field data on PANGAEA: ACLOUD AFLUX

1 Introduction

- Sea ice microwave emissivity highly variable in space and time
- Limits assimilation of passive microwave observations over sea ice [1]
- New ICI, MWS, and AWS partly sensitive to sea ice (Fig. 1)
- Sparse field data on sea ice emissivity above 200 GHz

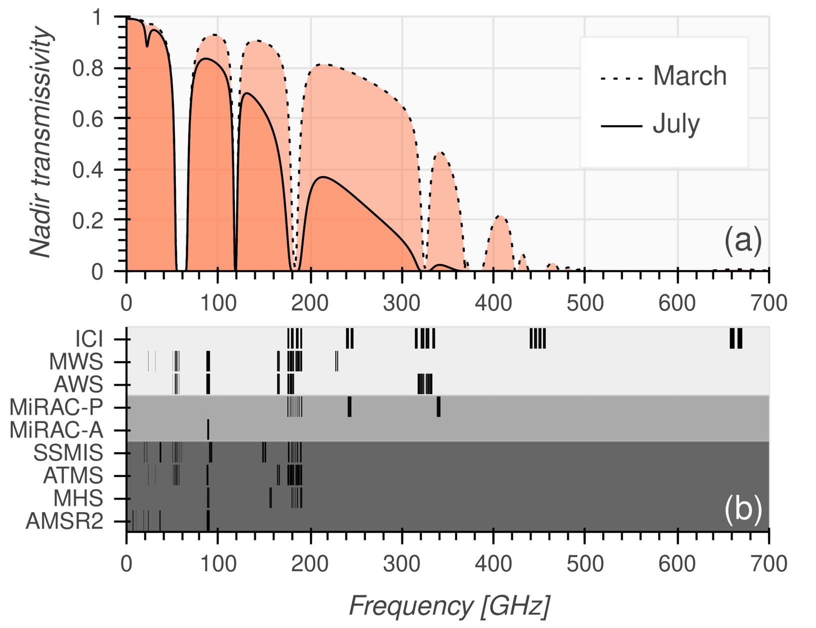

Fig. 1: (a) Nadir transmissivity at Ny-Ålesund (sounding data from [2]) and (b) instrument bandpasses.

Q1: Which sea ice properties affect the emissivity up to 340 GHz?
Q2: How do airborne observations compare with satellites?

2 Data

2.1 Field data

- ACLOUD (summer 2017) and AFLUX (spring 2019) airborne campaigns near Svalbard (Fig. 2) [3]
- MW radiometer MiRAC: 89h (25°), 183, 243, and 340 GHz (0°) [4]
- Matches with new satellite missions (Fig 1b)

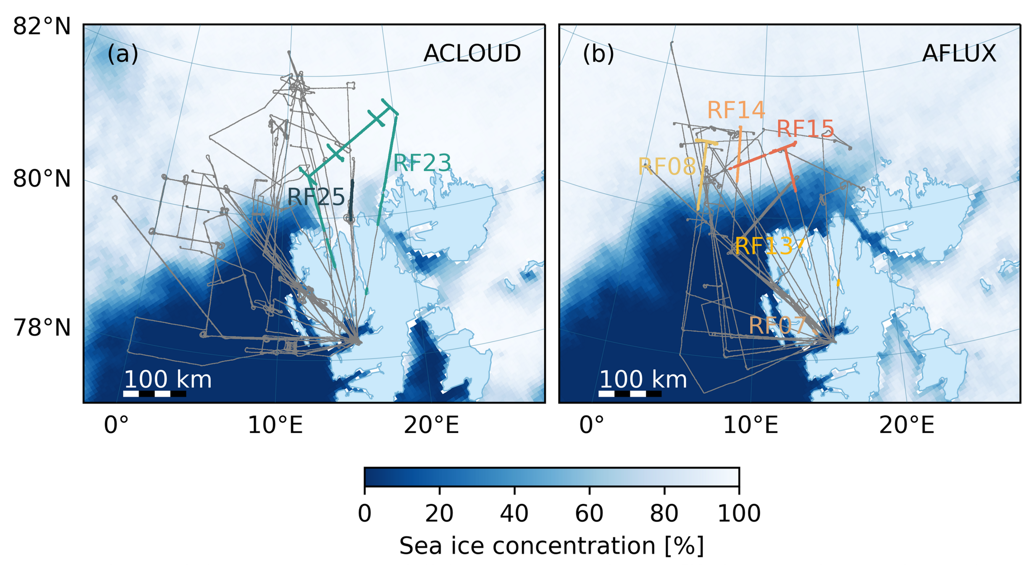

Fig. 2: (a) ACLOUD and (b) AFLUX Polar 5 flight tracks and sea ice concentration. Gray: all flights. Colored: emissivity segments.

2.2 Satellite data

- Inter-calibrated L1C Tb from NASA (V07) [5]:
  MHS on board Metop-A, -B, -C, NOAA-18, -19
  ATMS on board NPP, NOAA-20
  SSMIS on board DMSP-F16, -F17, -F18
  AMSR2 on board GCOM-W1
- Match with MiRAC at 89 and 183 GHz (Fig. 1b)

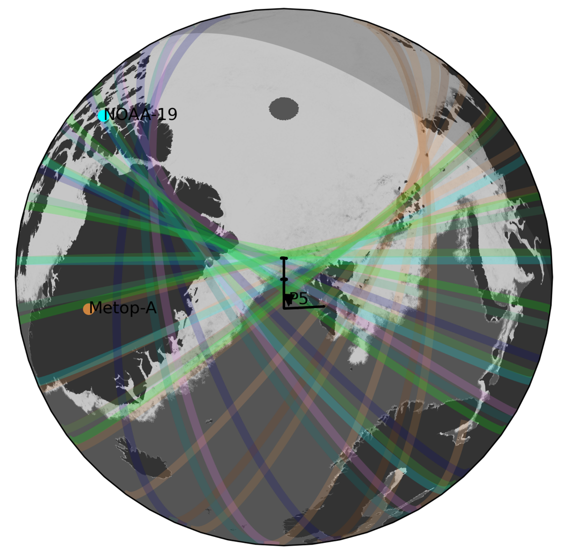

Fig. 3: Ground tracks within ±2 hours of the AFLUX RF08 clear-sky part in Fig. 2b.

3 Emissivity calculation

- Non-scattering RT equation solved for emissivity [6,7]:

$$Tb = e \cdot Ts \cdot t(0, h) + (1-e) \cdot Ta{\downarrow} \cdot t(0, h) + Ta{\uparrow}$$

- Atmospheric contribution simulated with the PAMTRA model [8]
- Dropspondes provide thermodynamic profiles
- Surface temperature from IR radiometer (aircraft) and L4 CMEMS sea ice surface temperature [9] (satellites)
- Surface reflection: Lambertian

4 Airborne emissivity

4.1 Histograms

- Warmer Tbs during ACLOUD than during AFLUX (Fig. 4, left)
- 89 GHz emissivity narrows from spring to summer (Fig. 4, right)
- Similar spring and summer emissivity at 183 and 243 GHz
- Two emissivity modes at 183, 243, and 340 GHz

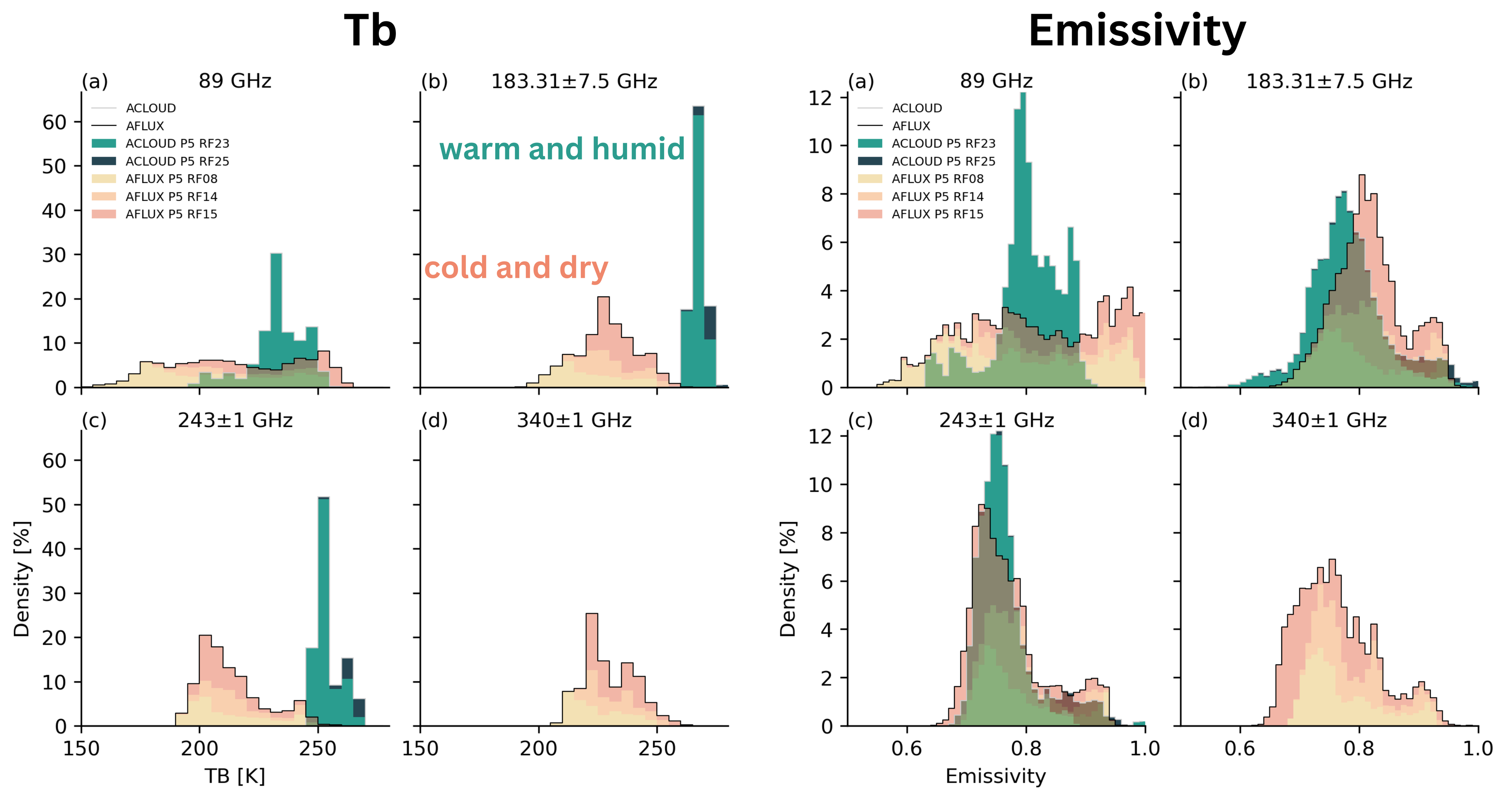

Fig. 4: Histograms of Tb (left) and emissivity (right) at (a) 89, (b) 183, (c) 243, and (d) 340 GHz during ACLOUD (gray line) and AFLUX (black line). Colors denote the relative contributions of individual research flights to the campaign histograms. The Tb (emissivity) bin width is 5 K (0.01). Observations under low surface sensitivity, i.e., at 340 GHz during ACLOUD, were excluded.

4.2 Influence of sea ice properties

- Grouped emissivity into four clusters with K-Means (Fig. 5a)
- Cluster properties: Surface temperature (Fig. 5b) and camera images (Fig. 6)
- Lower emissivity over compact sea ice
- Higher emissivity over young sea ice such as nilas

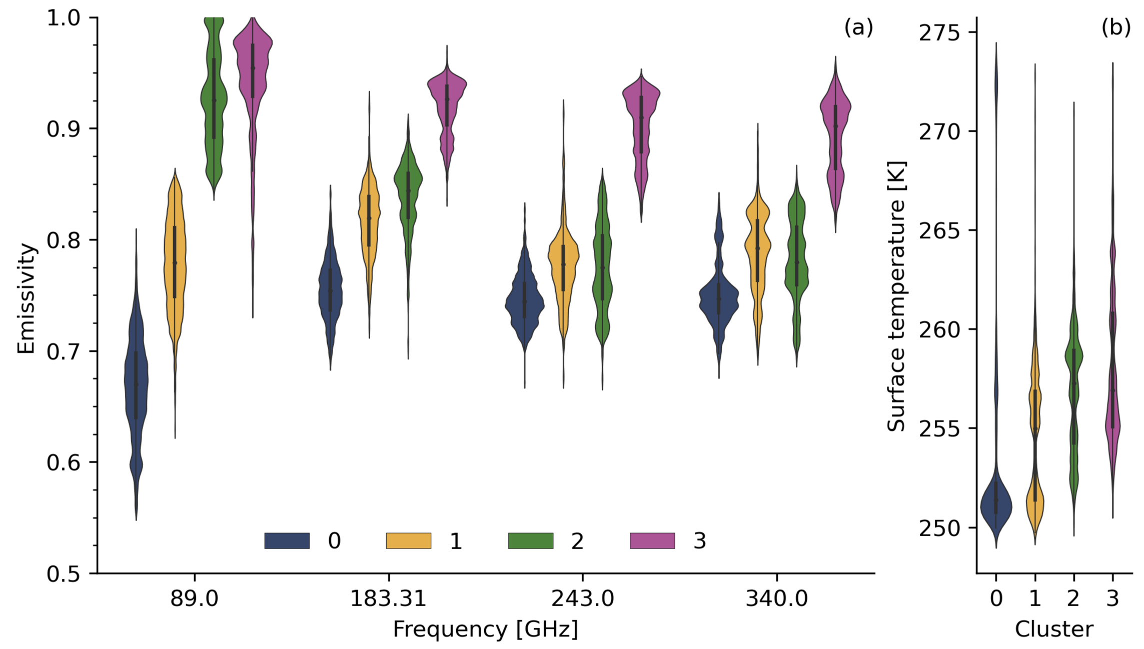

Fig. 5: Violin plots of the (a) emissivity at MiRAC frequencies and (b) surface temperature of the four K-Means clusters (colors).

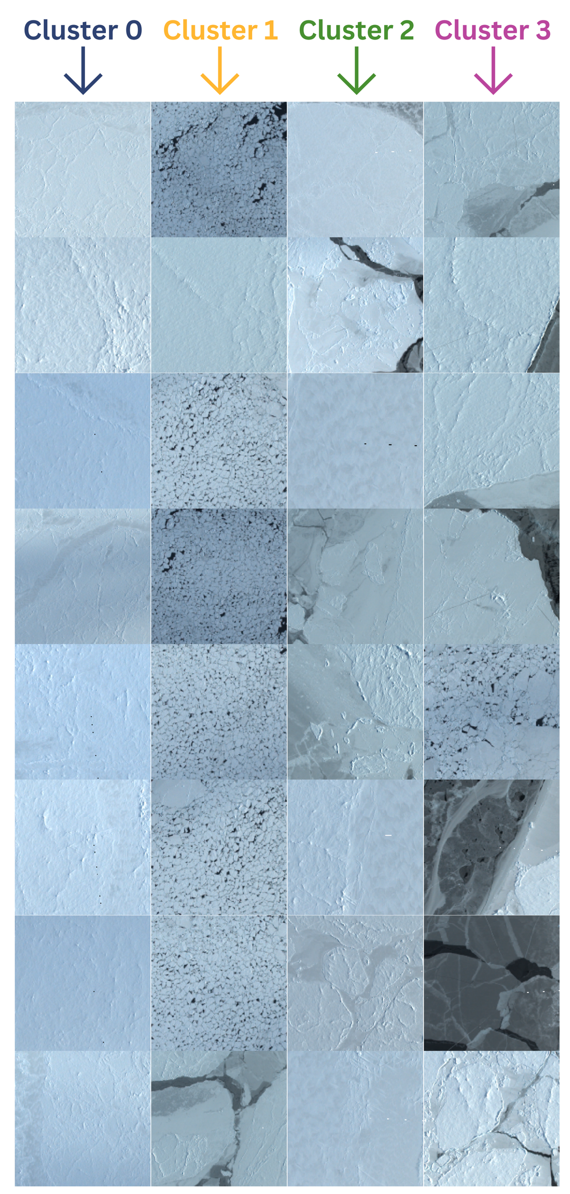

Fig. 6: Sea ice images closest to the cluster centroids.

5 Comparison with satellites

5.1 Spatio-temporal matching (here: MHS/ATMS)

- Collocated with satellites within ±2 hours
- Averaged to satellite resolution

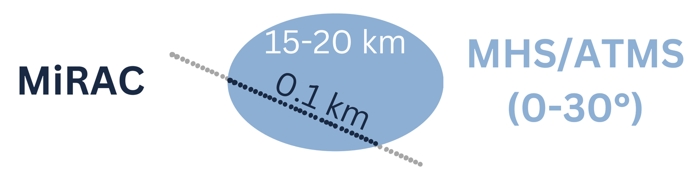

- MiRAC resolves emissivity features missed by satellites
- Limited bias at 183 GHz between both datasets (Fig. 7d)
- Partial footprint coverage causes emissivity differences

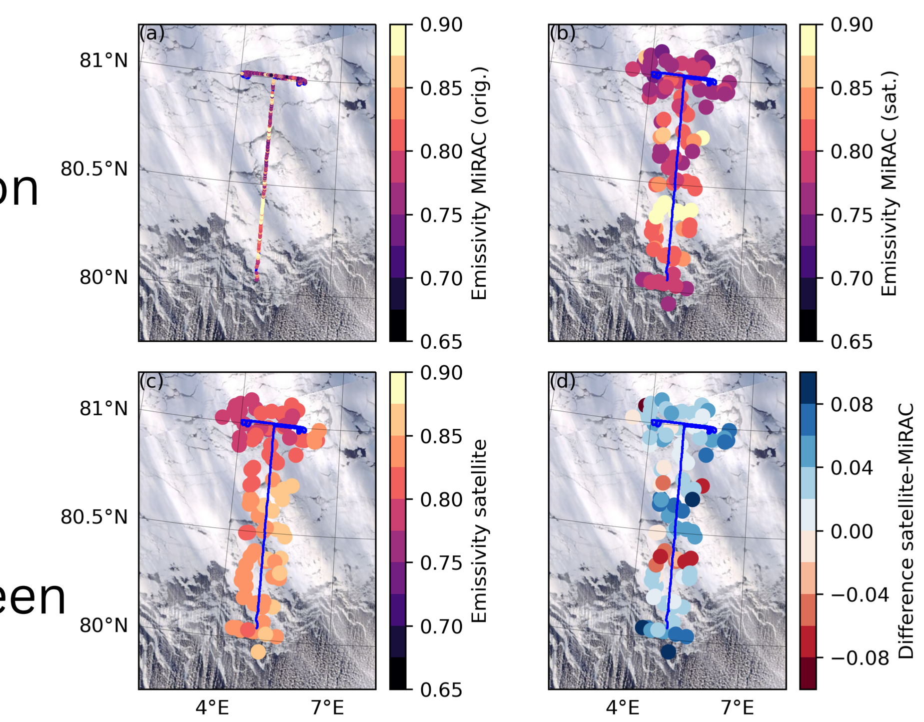

Fig. 7: Emissivity of (a) MiRAC at original and (b) satellite resolution and (c) MHS/ATMS and (d) their difference near 183 GHz during AFLUX RF08. Image: NASA Worldview.

5.2 Spectral emissivity variation

- Multi-channel and -platform emissivity distributions during AFLUX

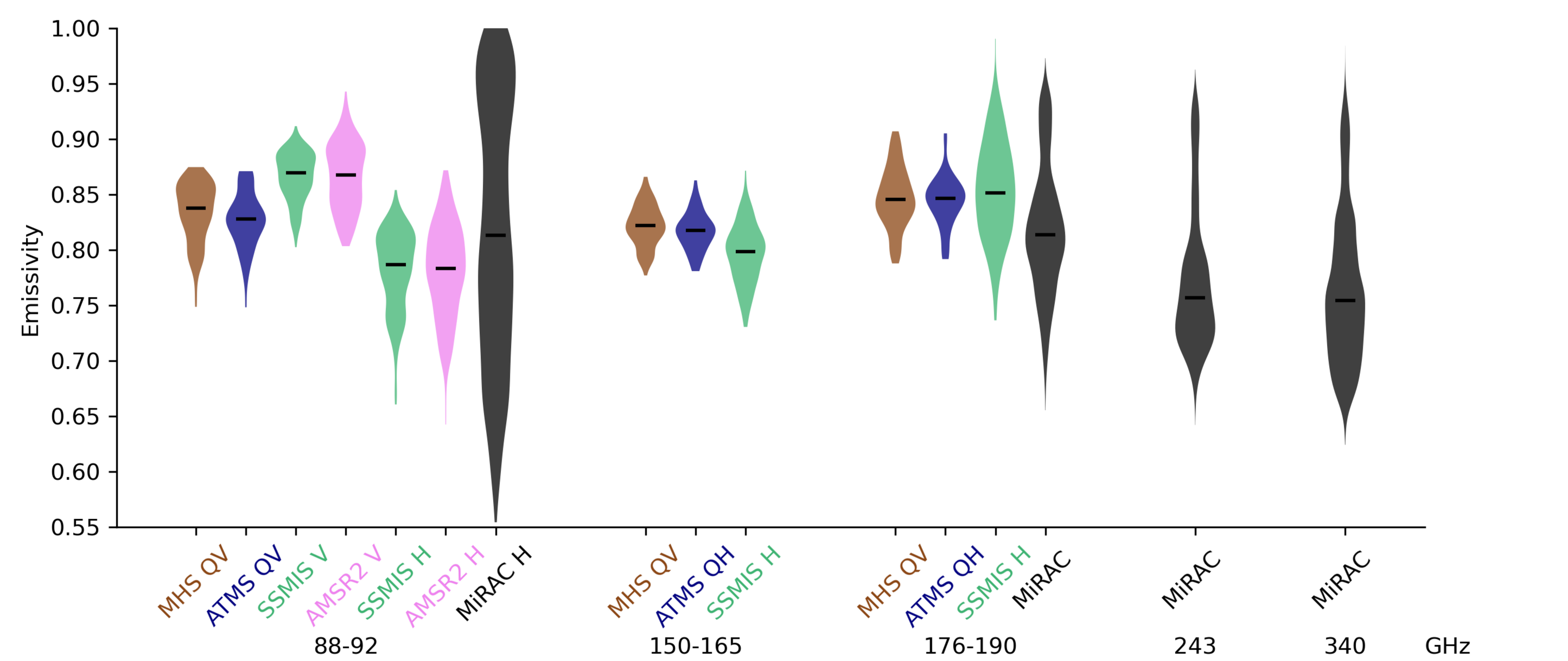

Fig. 8: Sea ice emissivity violin plots from satellites and MiRAC during AFLUX. Lines represent the median.

6 Conclusions

- Sea ice emissivity varies with ice type up to 340 GHz
- High frequencies behave similarly as assumed in TELSEM² [10]
- Field data matches spaceborne sensors at 89 and 183 GHz
- Downsampling provides 243 and 340 GHz emissivity at satellite resolution
- Useful for preparation for upcoming ICI, MWS, and AWS missions

7 References

[1] Lawrence, H et al. (2019). Quarterly J Royal Meteorol Soc 145(725): 3432-3454.
[2] Maturilli, M. (2020). PANGAEA (doi: 10.1594/PANGAEA.914973).
[3] Wendisch, M et al. (2023). Bull Am Meteorol Soc 104(1): E208-E242.
[4] Mech, M et al. (2019). Atmos Meas Tech 12(9): 5019–5037.
[5] Berg, W et al. (2016). J Atmos Ocean Technol 33(12): 2639-2654.
[6] Prigent, C et al. (1997). J Geophys Res 102: 21867–21890.
[7] Mathew, N et al. (2008). IEEE Trans Geosci Remote Sens 46(8): 2298–2306.
[8] Mech, M et al. (2020). Geosci Model Dev 13(9): 4229–4251.
[9] Nielsen-Englyst, P et al. (2023). Remote Sens Environ 284: 113331.
[10] Wang, D et al. (2017). J Atmos Ocean Technol 34(5): 1039–1059.

EGU General Assembly 2023, Vienna, Austria, 2023/04/23-28

Correspondence to: n.risse@uni-koeln.de